Small-angle neutron-scattering investigation of short-range correlations in fractal aerogels: Simulations and experiments

Anwar Hasmy, Marie Foret, Jacques Pelous, and Rémi Jullien
Laboratoire de Science des Matériaux Vitreux, Université Montpellier II, Place Eugène Bataillon, 34095 Montpellier Cedex 5, France
(Received 27 April 1993)

The center-to-center interparticle-distance distribution function $f(r)$ and its Fourier transform, the scattering function $S(q)$, are computed for simulated fractal aggregates made of identical spherical particles using several three-dimensional off-lattice cluster-cluster algorithms. As expected $f(r)$ exhibits a δ peak at the particle diameter followed by a discontinuity at twice this distance as a consequence of the nonoverlapping character of the spherical particles. As a result the curve $\log_{10}S(q)$ versus $\log_{10}q$ goes through a broad minimum followed by damped oscillations at large-q values. These simulations are compared with experimental small-angle neutron-scattering results on colloidal silica aerogels. The experimental scattering function $S(q)$ is derived from the ratio between the scattered intensity $I(q)$ and the form factor $P(q)$ determined from measurements on the diluted colloidal solution. The agreement between simulations and experiments is qualitatively good and the influence of aerogel density is well accounted for. The departure of the experimental curves from the theoretical $S(q)$ curve, which is stronger for larger particle sizes, is attributed to short-wavelength corrections to the simple scattering theory.

I. INTRODUCTION

Small-angle neutron scattering (SANS) as well as small-angle x-ray scattering are now used as a quite common tool[1-9] to determine the fractal dimension[10] of scale-invariant fractal aggregates.[11] The fractal character of the internal structure of an aggregate results in a power-law decay of the correlation function $f(r)$ and, as a consequence, in a linear dependence of the logarithmic of the scattered intensity $I(q)$ as a function of the logarithm of the modulus q of the scattering wave vector, which is given by

$$q=\frac{4\pi}{\lambda}\sin\frac{\theta}{2}\ , \tag{1}$$

where θ is the scattering angle and λ the wavelength of the incident beam. The linear regime is bounded by the Guinier regime[12] for q values of the order or smaller than ξ^{-1} where ξ is a typical upper cutoff and the Porod regime for q values of the order or larger than a^{-1} where a is the size of the subunits. The larger cutoff ξ relates to the typical size of the aggregates when one deals with diluted solutions of aggregates, such as aggregated sols: In this case the Guinier regime traduces the scattering by the aggregates. In the case of a concentrated distribution of connected aggregates, such as gels, ξ should be considered as the typical aggregate size, i.e., the mean connection length, because for distances larger than this length the medium appears to be homogeneous.

In this paper we focus on the large-q regime which is related to short interparticle distances within the aggregate. We have studied the crossover between the fractal and Porod regimes by both computer simulations and SANS experiments on colloidal aerogels. When the form factor of the individual particles is well defined, one can extract the precise form of the scattering function $S(q)$ from the intensity function $I(q)$. We show that all the short-range features of the correlation function, such as that revealed by computer simulations with standard cluster-cluster algorithms, are necessary to explain the full shape of the $S(q)$ curve at large-q values. The present analysis is more complete and more precise than earlier analyses that considered only part of these features (namely, the peak at the particle distance) and were obliged to consider an anomalously large number of neighbors to explain the experimental results.[4,12-14]

II. CLUSTER-CLUSTER ALGORITHMS

We have built three-dimensional aggregates, containing up to $N=4096$ particles, using several off-lattice hierarchical cluster-cluster computer algorithms.[11] We have considered three different aggregation mechanisms, namely, diffusion-limited,[15,16] ballistic,[17] and chemically limited[18] (also called reaction-limited[19]) processes. We review below the basis of these algorithms to show some details of the procedures used here which are different than the original ones. In this section we consider the case of "monodisperse" aggregates made of identical spheres of diameter a, conventionally taken as the unit length.

The hierarchical scheme is an iterative method which starts with a collection of $N_p=2^p$ identical spheres at iteration $i=0$ and ends with a unique aggregate of N_p particles at iteration p. At an intermediate iteration i, one has a collection of $N_c=2^{p-i}$ independent aggregates containing $N=2^i$ particles. To go to the next iteration, the 2^{p-i} aggregates are grouped into pairs and with each

pair we build a new aggregate according to a specific sticking rule. As soon as it is obtained, the new aggregate is randomly disoriented (using two successive random rotations about two randomly chosen coordinate axes) and is stored in the collection for the next iteration. The sticking rules depend on the chosen aggregation process. In the following the center of mass of an aggregate is denoted as G. The maximum radius R_m is defined as the maximum distance between the center of mass and the particle centers M_i and is given by

$$R_m = \max[GM_i] , \tag{2}$$

while the radius of gyration R_g is given by

$$R_g^2 = \frac{1}{N} \sum_{i=1}^{N} GM_i^2 . \tag{3}$$

A. Diffusion-limited case

The center of mass, $G(1)$, of one aggregate of the pair is placed at the origin of the coordinates and the center of mass, $G(2)$, of the other is placed on a point chosen at random on the sphere of radius

$$R_0 = R_m(1) + R_m(2) + a \tag{4}$$

centered at the origin. Then cluster (1) stays fixed and cluster (2) undergoes a random motion resulting from successive displacements of unit length chosen at random among the six coordinate directions $(\pm 1,0,0)$, $(0,\pm 1,0)$, $(0,0,\pm 1)$. The first time a particle C_2 of (2) overlaps a particle C_1 of (1), the Brownian motion is stopped and cluster (2) is translated in the opposite direction of the last displacement by the amount that makes a strict contact between C_1 and C_2. One should emphasize that, whereas the Brownian motion takes place on a cubic lattice the clusters themselves are built off lattice because the initial coordinates of $G(2)$ have no chance to be integers. As in the Witten-Sander model,[20] the Brownian motion is stopped when the distance $OG(2)$ becomes larger than a typical distance $R_M = 3R_0$ and cluster (2) is again released from the sphere of radius R_0 at a random position. This is repeated as often as necessary until an overlap occurs.

B. Ballistic case

As in the Brownian case, cluster (1) is fixed with $G(1)$ at the origin of the coordinates. A random straight line is determined by first choosing a random direction in space and then choosing a random point P in a plane perpendicular to this direction within a square limited by coordinates $(\pm R_0, \pm R_0)$ [R_0 being defined as in the diffusive case by Eq. (4)]. Then the center of mass of cluster (2) is moved along this straight line from an initial position such that $PG(2) = R_0$ toward cluster (1) until a first contact is made (the contract is determined in a manner similar to the last step of the Brownian motion in the diffusive case). If no contact is obtained, another random direction is chosen and the trials are repeated as often as necessary until a contact is obtained.

C. Chemically limited case

A particle of cluster (1) and a particle of cluster (2) are chosen at random as well as a random direction in space. The two clusters are disposed such that these two particles are in contact with their centers aligned along a random direction. Then a test of overlap is made for the other particles. If an overlap is found, the trial is discarded and another choice is made for both the particles and random direction.

In addition to the above procedures, we have also considered restructuration schemes, such as that described in Refs. 21 and 22 for the ballistic case. In this procedure three restructuring steps ($R_e = 1,2,3$) can be obtained. As soon as a contact occurs, a rotation is performed around an axis going through one contacting particle, say, C_1, and perpendicular to the linear trajectory, until a second contact is obtained. Among the two possible rotations, the one which corresponds to the smallest angle of rotation is chosen. This corresponds to one-step restructuring ($R_e = 1$). Calling K_1 and K_2 the centers of the new contacting particles, a further restructuring ($R_e = 2$) is obtained by rotating around C_1K_1 until a third contact is obtained (again with smallest angle). Sometimes new contacts may appear on the same particle so that further rotations can be performed as explained in Ref. 21. The three-step restructuring ($R_e = 3$) consists in achieving all the possible rotations.

For all the simulated aggregates, the fractal dimension D, as deduced from

$$N \sim R_g^D , \tag{5}$$

is reported in Table I.

Moreover, to illustrate this section, we give in Fig. 1 some three-dimensional pictures of aggregates containing 4096 particles. Case (a) corresponds to a ballistic aggregate without restructuring, while case (b) corresponds to the case of complete restructuring ($R_e = 3$). We do not show diffusion-limited and chemically limited aggregates, but they are very close to the one shown in Fig. 1(a). When comparing Figs. 1(a) and 1(b), one can observe the drastic compaction of the aggregate due to restructuring. However, since this compaction stays limited to short distances, the fractal dimension is not dramatically changed (see Table I). For comparison, we show in Fig. 1(c) a micrograph of an aerogel sample that we will discuss in Sec. V.

TABLE I. Fractal dimensions D and coordination numbers z of the aggregates built with diffusion-limited (A), ballistic (B), chemically limited (C) as well as restructured ($R_e = 1,2,3$) algorithms. D is estimated from the radius of gyration [formula (5)], and D^* is estimated from the slope of the $\log_{10}S(q)$ vs $\log_{10}q$ curve in the linear regime. In both cases the uncertainties originating from the fit are estimated to be of order 0.03.

	A	B	C	$R_e=1$	$R_e=2$	$R_e=3$
D	1.78	1.95	2.04	2.13	2.18	2.19
D^*	1.72	1.88	1.96	2.12	2.14	2.16
z	2.0	2.0	2.0	3.6	4.4	5.1

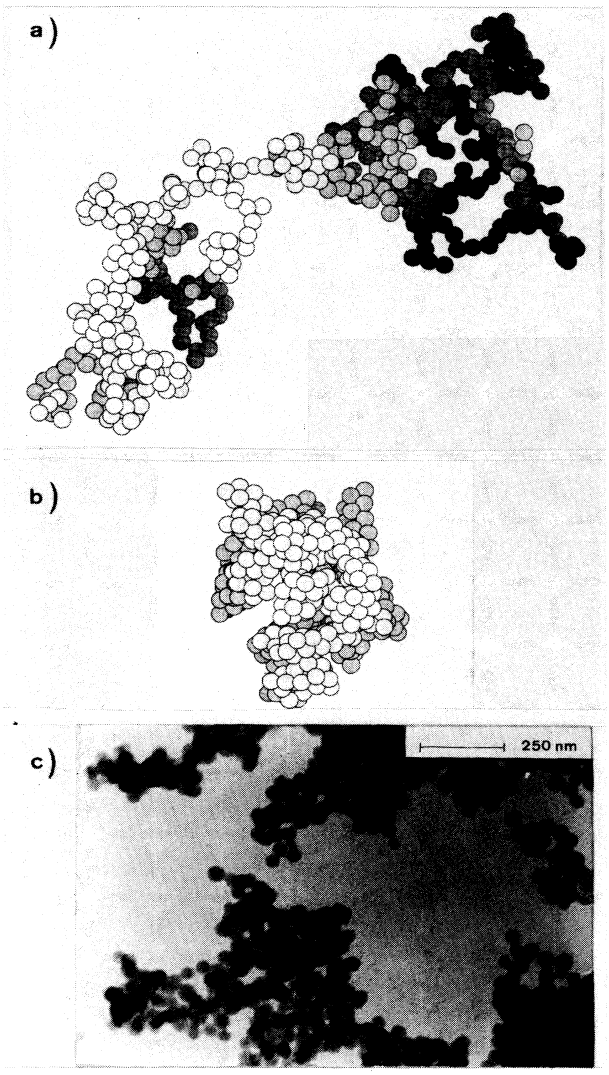

FIG. 1. (a) Three-dimensional aggregate containing 4096 spherical particles built with the ballistic algorithm without restructuring. (b) Same as (a) but with complete restructuring ($R_e=3$). (c) Micrograph of a 270-Å aerogel sample.

III. CALCULATION OF THE DISTANCE DISTRIBUTION FUNCTION $f(r)$

An aggregate containing N particles being given by the set of coordinates for the centers M_i of its particles, one can calculate its distance distribution function $f(r)$, which is the histogram of center-to-center distances M_iM_j. Here we have chosen to calculate the distance distribution function per particle so that $f(r)$ is normalized by

$$\int_0^\infty f(r)4\pi r^2 dr=\frac{N-1}{2} . \tag{6}$$

In practice, after choosing a given path δr, one calculates the number of distances M_iM_j lying in the interval $[r-\frac{1}{2}\delta r, r+\frac{1}{2}\delta r]$, and to find $f(r)$, one divides the result by $4N\pi r^2\delta r$.

One should point out that $f(r)$, which is defined here for a unique aggregate, differs from the usual correlation function $g(r)$ for a gel, which is generally considered as a collection of connected aggregates. The difference occurs at large distances ($r>\xi$) where $f(r)$ tends to zero in our case while $g(r)$ tends to a constant g_∞ proportional to the gel density, in the other case. Usually, $g(r)$ is normalized such that $g_\infty=1$. It is generally admitted that in a gel the short-range correlation contributions, due to the constitutive connected aggregates of typical size ξ, are added to a uniform background given by g_∞ so that our $f(r)$ should be proportional to $g(r)-1$.

The numerical results for $f(r)$ are reported in Figs. 2(a) and 2(b) for aggregates containing $N=4096$ parti-

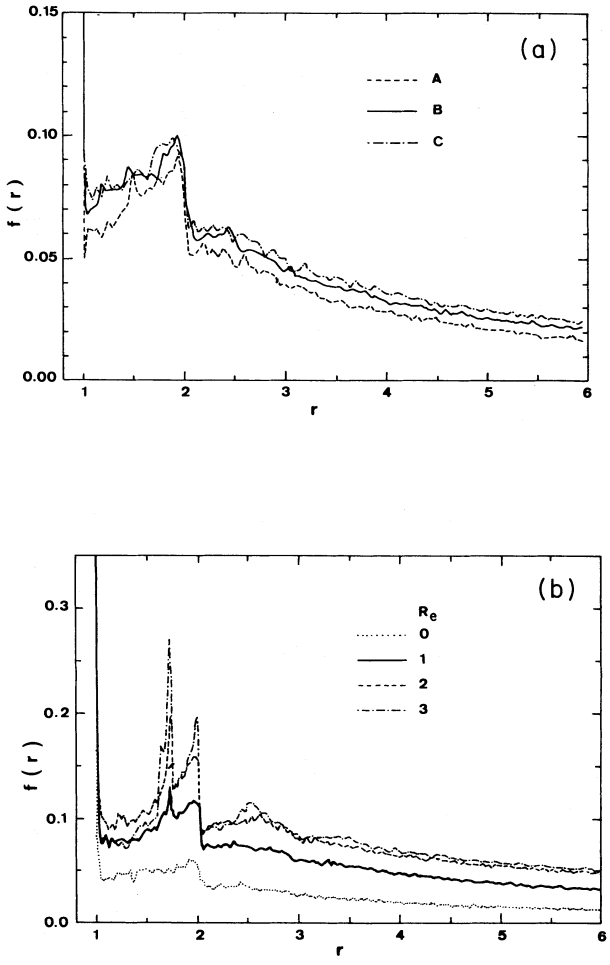

FIG. 2. (a) Numerical results for the distance distribution function $f(r)$ (calculated with $\delta r=0.03$) in the case of aggregates containing $N=4096$ particles. Curves A, B, and C refer to diffusion-limited, ballistic, and chemically limited algorithms, respectively. (b) Same as in (a) but with different degrees of restructuring ($R_e=0,1,2,3$) included in the ballistic algorithm.

cles, with $\delta r=0.03$. In Fig. 2(a) the three curves A, B, and C correspond to the diffusion-limited, ballistic, chemically limited cases, respectively. In Fig. 2(b) the curve for a nonrestructured ballistic aggregate ($R_e=0$) is compared with those corresponding to different steps of restructuring ($R_e=1,2,3$). A curve similar to the one reported in Fig. 2(a), but computed with a larger δr, has already been obtained by Meakin for a diffusion-limited aggregate as quoted in Ref. 13. However, this curve has not been used to calculate the scattering function.

In all cases one observes a strong peak at $r=1$ and a discontinuity at $r=2$. Above these short-range features, say for distances larger than 2.5, $f(r)$ follows quite well the power-law behavior

$$f(r)=Ar^{-(3-D)} \tag{7}$$

that is expected from the fractal character of the aggregates. The upper limit of the power-law regime, where $f(r)$ tends to zero, is outside the limit of the figures since ξ is quite large here. From the normalization condition (7) and if one forgets the small- and large-r contributions to the integral, the coefficient A should be roughly proportional to $D-1$. This is quite well observed in the figures where the curves of larger D are above the curves of smaller D.

The strong peak at $r=1$ is due to the nonzero number of distances $r=1$ corresponding to bonds between contacting particles. Introducing the coordination number z, which is the average number of contacts per particle, the total number of contacts is zN, and since there are two contacts per bond, the total number of bonds is $zN/2$. As a consequence, one gets

$$f(1)=\frac{z}{8\pi\delta r} , \tag{8}$$

and since z is nonzero, this quantity tends to infinity when δr tends to zero. Thus, in the asymptotic limit ($N\rightarrow\infty$), $f(r)$ contains a δ peak of weight $z/8\pi$ at $r=1$. In the nonrestructured case, since one starts with individual particles and one adds one bond per sticking, the resulting cluster has no loop and the total number of bonds is $N-1$. In this case one has

$$z=2\left[1-\frac{1}{N}\right]\simeq 2 . \tag{9}$$

We have calculated z directly, and we have checked this formula in the case of nonrestructured aggregates. The values of z in the restructured cases are reported in Table I. Values of z larger than 2 are due to the formation of quite compact subunits in the early iterations. For $R_e=3$, one systematically builds regular tetrahedra at iteration 2 and then the resulting large aggregates are made of tetrahedral subunits connected together by at least three bonds.

Both the nonzero value of $f(r)$ for $r=1+$ and the discontinuity at $r=2$ can be understood if one considers that $f(r)$ can be written as

$$f(r)=f_1(r)+f_2(r) , \tag{10}$$

where $f_1(r)$ is the contribution of couples of particles that are tangent to the same third one and where $f_2(r)$ contains all the other contributions. We have observed that, while $f_2(r)$ is continuously varying from $r=1$, where $f_2(1)=0$, up to the largest distance, going through a maximum around $r=2$, $f_1(r)$ exists only between $r=1$ and 2 and reaches nonzero values at both limits. An approximation $f_a(r)$ of $f_1(r)$ can be calculated by assuming that the oriented bonds $\overrightarrow{M_0M_1}$ and $\overrightarrow{M_1M_2}$ that connect two particles M_1 and M_2 to a third one M_0 make an angle θ that is randomly distributed between 0 and $2\pi/3$, with a constant probability distribution $p(\theta)=p_0$. One can calculate p_0 by

$$2\pi\int_0^{2\pi/3}p_0\sin\theta\,d\theta=1 , \tag{11}$$

giving

$$p_0=\frac{1}{3\pi} . \tag{12}$$

Then, knowing that

$$r=2\cos\frac{\theta}{2} , \tag{13}$$

one writes

$$4\pi r^2 f_a(r)dr=|2\pi p_0\sin\theta\,d\theta| \tag{14}$$

and finds

$$f_a(r)=\frac{1}{6\pi r} . \tag{15}$$

With this approximation $f(1+)$ should be equal to $1/6\pi=0.055\ldots$ and the discontinuity $\Delta f=f(2-)-f(2+)$ should be equal to $\frac{1}{2}f(1+)=0.027\ldots$. In our calculations with nonrestructured aggregates, we find $f(1+)$ ranging from 0.055 to 0.075 and Δf ranging from 0.03 to 0.04, values of the same order of magnitude but slightly larger than the predicted values. The discrepancies can be attributed to the approximation made: It is clear that $p(\theta)$ is not constant for two reasons. First, there may be other particles in the close neighborhood affecting the possible configurations of the three particles M_0, M_1, and M_2 (this occurs in particular if M_0 has three or more contacts). Second, in the diffusion-limited and ballistic cases, screening effects imply that small values of θ are favored.

When restructuring is introduced, some other short-range features show up in the $f(r)$ curve. As soon as $R_e\neq 0$, it appears as a peak at $r=\sqrt{3}$. This peak is due to the contribution of particles that are connected with two bonds to the same dimer of tangent particles, and it can be accounted for by a similar reasoning as above. The only difference lies in the fact that the maximum distance is here obtained in a plane rather than in space, so that the peak is a weak divergency of the kind $(\sqrt{3}-r)^{-1/2}$ rather than a discontinuity. Moreover, for $R_e=3$, one observes a peak at $2\sqrt{\frac{2}{3}}$, which is twice the height of the tetrahedral subunit. If one forgets the general long-range decrease of $f(r)$ due to the fractal character of the aggregates, the overall shape of $f(r)$, which ex-

hibits damped oscillations at $r > 2$, becomes, for large R_e values, qualitatively similar to the shape of the correlation function for random packings of spheres.[23]

IV. CALCULATION OF THE SIMULATED SCATTERING FUNCTION $S(q)$

The scattering function $S(q)$ of an aggregate corresponds to the scattering intensity of dimensionless points located at its particle centers M_i. With a convenient normalization, $S(q)$ is given by

$$S(q)=\frac{1}{N}\left|\sum_{i=1}^{N} e^{i\mathbf{q}\cdot\mathbf{r}_i}\right|^2=\frac{1}{N}\sum_{i,j} e^{i\mathbf{q}\cdot(\mathbf{r}_i-\mathbf{r}_j)} , \tag{16}$$

where $\mathbf{r}_i=\overrightarrow{\mathbf{OM}}_i$. Assuming that the aggregate is spherically symmetric, one can average over the directions of $\mathbf{q}$ to find

$$S(q)=\frac{1}{N}\sum_{i,j}\frac{\sin qr_{ij}}{qr_{ij}} , \tag{17}$$

with

$$r_{ij}=M_iM_j=|\mathbf{r}_i-\mathbf{r}_j| . \tag{18}$$

Considering separately the contributions $i=j$ and $i\neq j$, one gets

$$S(q)=1+\frac{1}{N}\sum_{i\neq j}\frac{\sin qr_{ij}}{qr_{ij}} . \tag{19}$$

Then, using the distribution of distances $f(r)$ as defined above,

$$S(q)=1+2\int_0^{\infty}\frac{\sin qr}{q}4\pi r f(r)dr , \tag{20}$$

the normalization conditions imply that

$$S(0)=N \quad \text{and} \quad S(\infty)=1 . \tag{21}$$

In practice, to avoid numerical imprecisions, we have preferred to calculate $S(q)$ directly by the double sum (19) rather than by the Fourier transform of $f(r)$ given by (20).

We give the results of the calculations in Fig. 3. In Fig. 3(a), we have plotted $\log_{10}S(q)$ as a function of $\log_{10}q$ in the diffusion-limited case for $N=4096$, emphasizing the range of large-q values. In this figure one observes a large minimum at about $q\simeq 4$ followed by damped oscillations. The oscillations can be attributed to the δ peak

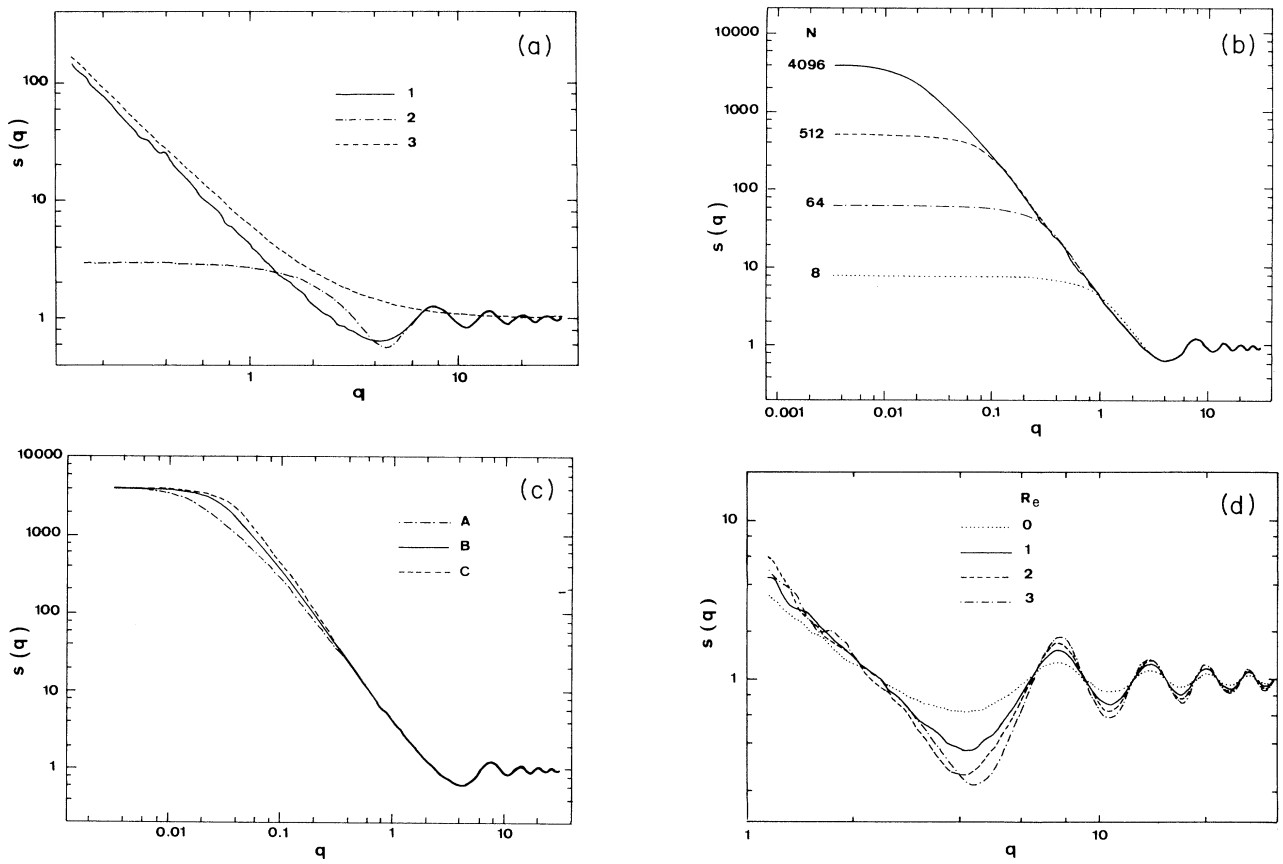

FIG. 3. (a) Numerical results for the scattering function $S(q)$. Curve 1 corresponds to a diffusion-limited aggregate with $N=4096$ particles, and curves 2 and 3 correspond to the analytical formulas (22) and (24), respectively. (b) $S(q)$ curves for diffusion-limited aggregates with different N values. (c) $S(q)$ curves for different aggregation mechanisms. Curves A, B, and C correspond to diffusion-limited, ballistic, chemically limited aggregates of $N=4096$ particles, respectively. (d) $S(q)$ curves for ballistic aggregates of $N=4096$ particles with different degrees of restructuring.

of $f(r)$. If one substitutes, in (20), $f(r)$ by $(z/8\pi)\delta(r-1)$, one gets the following approximate for $S(q)$:

$$S_\infty(q)=1+z\frac{\sin q}{q} , \tag{22}$$

which is represented, for $z=2$, by curve 2 in Fig. 3(a). As expected, this approximation corresponds to the asymptotic large-q limit of $S(q)$. However, the large minimum at $q\simeq 4$ is not accounted for by this contribution only. Both the δ peak at $r=1$ and the discontinuity at $r=2$ influence the shape of the first minimum of $S(q)$. It is interesting to compare our results with an analytical formula which has been widely used in the literature:[4,5,13]

$$S(q)=1+\frac{D2^D\Gamma(D-1)}{q^D}\frac{\sin[(D-1)\tan^{-1}(q\xi/a)]}{[1+(a/q\xi)^2]^{(D-1)/2}} . \tag{23}$$

In the range of q values depicted in Fig. 3(a), the precise value of ξ has no influence and here we have considered the limit $\xi\rightarrow\infty$ given by

$$S(q)=1+\frac{D2^D\Gamma(D-1)}{q^D}\sin\frac{(D-1)\pi}{2} . \tag{24}$$

We have taken $D=1.75$ as in the diffusion-limited case. Since formula (24) does not take into account any short-range hard-core effects, it cannot account for the oscillations observed in $S(q)$. In practice, as seen in Fig. 3(a), our $S(q)$ curve (curve 1) crosses over from curve 3 in the fractal regime ($q<1$) to curve 2 in the large-q regime ($q>10$).

In Fig. 3(b) we show several $S(q)$ curves for different values of N in the diffusion-limited case. As expected, the range of the fractal region is reduced for smaller aggregates, but the large minimum and the damped oscillations are independent of size up to very small sizes, showing that the short-distance correlations are fixed by the early stages of the aggregation process. In Fig. 3(c) we have plotted $\log_{10}S(q)$ as a function of $\log_{10}q$ for $N=4096$ in the three different cases: diffusion-limited, ballistic, and chemically limited. In this figure one can see the change of slope in the fractal regime due to the influence of the fractal dimension, but after this regime, one sees that the overall shape of $S(q)$ is quite independent of the aggregation process. This means that the mean shapes of the small clusters built in the early stages are very close from one aggregation process to another. In particular, their coordination number is the same ($z=2$). In Fig. 3(d) we give the same plot, but in the ballistic case only, for different steps of restructuring. One sees that, in presence of restructuring, the minimum is deeper and narrower. This clearly shows the influence of the coordination number z, which is now increasing with R_e. The fractal dimensions D^* estimated from the slope of the $S(q)$ curves of Figs. 3(c) and 3(d) have been reported in Figs. 1 and 2. Although D^* is systematically smaller than D, the difference is not significative since it remains of the order of the error bar.

V. COMPARISON WITH SANS EXPERIMENTS ON SILICA AEROGELS

The aerogels have been prepared using the process described in Ref. 14. They have densities ranging from 0.070 to 0.380 g/cm^3. They are made of small colloidal spherical particles with a quite low diameter polydispersity as has been checked on electron micrographs such as Fig. 1(c). The particle diameter a ranges from 96 to 270 Å. Hereafter, samples will be referred to by their particle diameters. Figure 4(a) shows a typical intensity curve obtained with one 270-Å aerogel. In this figure $\log_{10}I(Q)$ has been plotted as a function of $\log_{10}Q$. Here we use a different notation for the experimental wave vector Q (measured in Å^{-1}) and for the dimensionless one $q=Qa$ that we have used above. One clearly see in this figure the characteristic Q^{-4} Porod behavior with strong oscillations. As usual, we analyze the intensity in terms of two factors:

$$I(Q)=NS(Q)P(Q) , \tag{25}$$

where $S(Q)$ is the scattering function introduced above and where $P(Q)$ is the form factor, i.e., the scattering intensity for a spherical particle alone. For an homogeneous sphere of diameter a, $P(Q)$ is given by

$$P(Q)=v^2\left[3\frac{\sin(Qa/2)-(Qa/2)\cos(Qa/2)}{(Qa/2)^3}\right]^2 , \tag{26}$$

where v is the volume of the sphere:

$$v=\frac{\pi}{6}a^3 . \tag{27}$$

To account for the finite values of the minima of $I(Q)$, one must consider a small polydispersity of the particle diameters. Consequently, we have replaced $P(Q)$ by an average $\overline{P(Q)}$ over the diameters,

$$\overline{P(Q)}=\int_0^\infty P(Q)g(a)da , \tag{28}$$

according to a Gaussian probability distribution:

$$g(a)\sim\exp\left[-\frac{1}{2}\left[\frac{a-a_0}{\sigma}\right]^2\right] , \tag{29}$$

which has been truncated for $a<0$ and normalized accordingly.

In Fig. 4(a) the solid line represents $\overline{P(Q)}$ for $a_0=270$ Å and $\sigma=32$ Å. The parameters a_0 and σ have been adjusted in order to get the best fit between $\overline{P(Q)}$ and the intensity scattered from the diluted sol in which the silica particles can be assumed to scatter neutrons independently. The discrepancy at very-small-Q values can be attributed to some long-range organization of the colloidal particles in the sol. One can check that the same solid line fits the large-Q part of the corresponding $I(Q)$ curve up to the largest available Q values. The value of a_0 is mainly determined by the location of the minima and σ by their absolute values. The absolute error on the values of both a_0 and σ is estimated to be of order 5 Å. The same analysis has been done for all our experimental

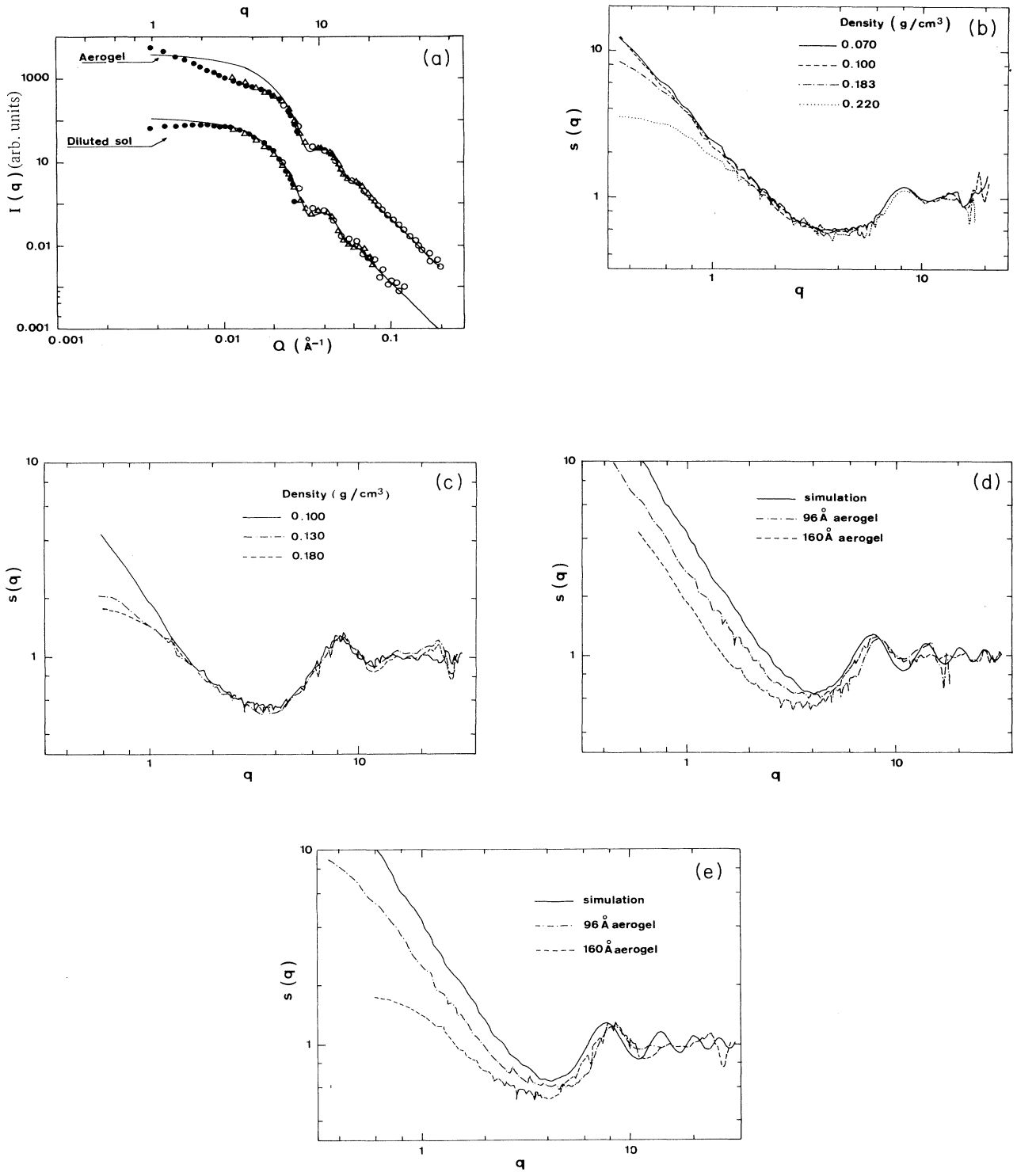

FIG. 4. (a) SANS intensity for one 270-Å aerogel (upper curve) and for the corresponding diluted sol (lower curve). The solid line is a fit of the lower curve to Eq. (28) as explained in text. The different symbols refer to distinct configurations of the spectrometer. (b) Experimental $S(q)$ curves (obtained as explained in text) for the 96-Å aerogel family. Samples are labeled by their densities. (c) Experimental $S(q)$ curves for the 160-Å family. (d) Experimental $S(q)$ curves for samples of various particle diameters but with the same density $\rho=0.10$ g/cm^3 and the simulated $S(q)$ curve in the diffusion-limited case. (e) Same as (d) for $\rho=0.18$ g/cm^3.

data, and in the following we give the results for the scattering function as being the ratio of $I(Q)$ by $\overline{P(Q)}$ as a function of the reduced wave vector $q=Qa_0$. All the experimental $S(q)$ curves, determined this way, have been normalized such that $S(q)\rightarrow 1$ for $q\rightarrow\infty$. Justifications for the use of formula (25) in presence of polydispersity are given in the Appendix.

In Fig. 4(b) we give $\log_{10}S(q)$ versus $\log_{10}q$ for different aerogels made of particles of the same size ($a_0=96$ Å) but with densities ranging from 0.070 to 0.250 g/cm^3. In this figure one observes the same characteristic broad minimum followed by damped oscillations that we have observed in the simulated curves. The fact that all the curves are superimposed in the fractal regime as well as in the large-q region gives good confidence that the aggregates forming the gel have been grown with the same aggregation process. The fractal dimension is here $D=1.80$. Moreover, one clearly sees in this figure that the density fixes the size ξ of the aggregates constituting the gel. However, no further quantitative comparison between simulation and experiment can be done here. In particular, an estimation of the number of particles N based on the use of Fig. 4(b) would have no meaning, because the simulation has been done with one single aggregate containing a given number N of particles, while the gel is made of a collection of connected blobs of various sizes. In Fig. 4(c) the same kinds of plots have been depicted for larger particles ($a_0=160$ Å). Here also the curves are nicely superimposed for large-q values and exhibit the predicted overall shape.

In Fig. 4(d) we compare two experimental $S(q)$ curves for the same aerogel density ($\rho=0.10$ g/cm^3) with the simulated curve in the diffusion-limited case (with $N=4096$). The same has been done in Fig. 4(e), but for a different density ($\rho=0.18$ g/cm^3). It is clear in these two figures that the agreement between theory and experiments is only qualitative. Even if the data are very noisy for large-q values, it seems that the large-q oscillations of the experimental curves are more damped. This may be accounted for by taking into account indirectly the diameter polydispersity into $S(q)$ as is demonstrated in the Appendix (see Fig. 5). But we would like to focus on the larger discrepancy, which is that the minimum is wider and deeper in the experimental curves. This discrepancy is systematically more important for bigger particles. When comparing with Fig. 3(d), it is clear that this cannot be attributed to the kind of restructuring that we have considered at the end of Sec. II, since for such restructuring the minimum is deeper but not wider. Since it is difficult to imagine some other realistic restructuring mechanisms able to fully account for the observed discrepancies, we do not trust the earlier interpretations which considered quite large coordination numbers.[4,12–14] One might invoke other possible explanations for the discrepancies such as small-q modifications of the form factor or corrections to the scattered intensity due to some shape deformation of the particles near their contact zone. This last effect might be approximately taken into account by considering a different length for the particle diameter and for the center-to-center distance between contacting particles. However, all these considerations, if they might sometimes give a better fit, appear to be too *ad hoc* to really improve comprehension of the problem.

Here we would like to propose another tentative interpretation. In general, a complete theory of scattering (including multiple scattering, shadowing, refraction, etc.) should consider two dimensionless parameters Qa and $ka=2\pi a/\lambda$. The fact that the theoretical $S(q)$ curve considered above does not depend on the extra parameter ka comes from all the considered approximations. However, the simple scattering theory should be recovered in the limit $ka\rightarrow 0$. Some corrections might appear for large-ka values. The fact that in Figs. 4(d) and 4(e) the theoretical curve can be considered as the limit of the experimental ones when $a\rightarrow 0$ supports this analysis. Moreover, the parameter ka is quite large in our case. We used a combination of two incident neutron wavelengths of 6 and 18 Å in the experimental setup. Thus our ka values are in the range 30–300, close to the values involved in the geometrical optics approximation. It is reasonable to admit that corrections to the simple scattering theory, such as shadowing, refraction, and multiple scattering effects, cannot be neglected for such large values. Theoretical calculations are under progress to try to give more validity to this reasoning.

VI. CONCLUSION

In this paper we have shown that the shape of the experimental scattering curve for large wavelength values in colloidal aerogels is qualitatively well reproduced by direct calculations on simulated aggregates built with cluster-cluster algorithms. In a log-log plot, the scattering curve exhibits a broad minimum followed by damped oscillations at large-q values. We have shown that it is not necessary to consider anomalously large coordination numbers to explain the experimental curves as was previously done. The discrepancies that we obtain between experiments and theory are here attributed to corrections to the simple scattering theory in the limit of small wavelengths. The present investigation will be soon completed in the small-q regime by a study of the long-range correlations by means of both simulation calculations and experiments. In this limit the calculations are more complicated since one must consider scattering by a set of connected aggregates disposed in a manner which should be sufficiently realistic to correctly model the structure of aerogels.

APPENDIX

To justify the analysis of the experimental results done in Sec. V, we have built polydisperse diffusion-limited aggregates. This calculation has been done by extending straightforwardly the hierarchical procedure described in Sec. II. Now we start the simulation with a collection of spherical particles whose diameters a are given by

$$a=a_0+2\sigma\left[\frac{3}{n}\right]^{1/2}\sum_{k=1}^{n}\left[\xi_k-\frac{1}{2}\right], \tag{A1}$$

where n is an integer and the ξ_k's are independent ran-

dom variables uniformly distributed between 0 and 1 as given by our computer random generator. It is known that this distribution tends to the Gaussian distribution of mean a_0 and standard deviation σ in the limit $n \to \infty$. In practice, it is not necessary to consider a very large value of n to have a good approximation of the Gaussian distribution, and here we have taken $n=5$. At the end of the procedure, we have stored the coordinates of the particle positions r_i as well as their diameters a_i.

Then, given the aggregate, the scattered amplitude $A(Q)$ can be calculated by

$$A(Q)=\sum_i e^{iQ\cdot r_i}\int_{v_i} e^{iQ\cdot\rho_i}d^3\rho_i \ , \tag{A2}$$

where the integral is performed over the volume v_i of the ith particle. Using

$$b(Q,a_i)=\int_{v_i} e^{iQ\cdot\rho_i}d^3\rho_i$$
$$=4\pi a_i^3\frac{\sin Qa_i/2-Q(a_i/2)\cos Qa_i/2}{(Qa_i)^3} \tag{A3}$$

and making the average over the direction of Q, the scattering intensity is

$$I(Q)=|A(Q)|^2=\sum_{i,j} b(Q,a_i)b(Q,a_j)\frac{\sin Qr_{ij}}{Qr_{ij}} \ . \tag{A4}$$

It can be checked that this formula reduces to (25) and (26) in the monodisperse case. However, in general, one cannot write $I(Q)$ under the form of a product as in (25).

We have calculated $I(Q)$ with formula (A4), and we have divided it by an averaged form factor $\overline{P(Q)}$ calculated as in (26)–(28) but with the distribution of diameters defined by (A1). This procedure gives a pseudoscattering function $S(\widetilde{Q})$:

$$S(\widetilde{Q})=\frac{I(Q)}{N\overline{P(Q)}} \ , \tag{A5}$$

which we compare with the monodisperse $S(Q)$ curve in Fig. 5.

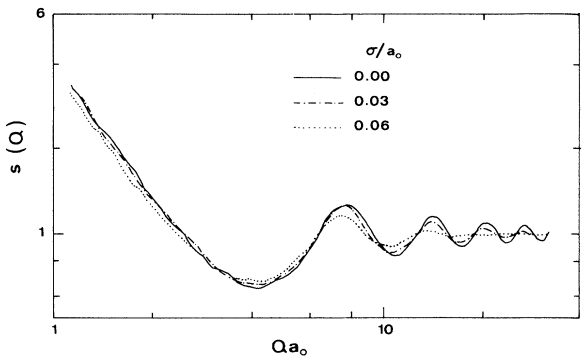

FIG. 5. Numerical results for the scattering function $S(Q)$ of a monodisperse aggregate compared with the approximate function $S(\widetilde{Q})$ obtained by dividing $I(Q)$ calculated for a polydisperse aggregate by an averaged form factor $\overline{P(Q)}$. The polydisperse aggregate contains $N=4096$ particles. The standard deviations of the diameters are $\sigma=0.03a_0$ and $0.06a_0$.

One can see that the agreement is quite good. The differences occur for large-Q values where the oscillations become more and more damped when σ increases.

[1]D. W. Schaefer, J. E. Martin, P. Wiltzius, and D. S. Cannell, Phys. Rev. Lett. **52**, 2371 (1984).
[2]M. Axelos, D. Tchoubar, and R. Jullien, J. Phys. (Paris) **47**, 1843 (1986).
[3]T. Freltoft, J. K. Kjems, and S. K. Sinha, Phys. Rev. B **33**, 269 (1986).
[4]P. Dimon, S. K. Sinha, D. A. Weitz, C. R. Safinya, G. Smith, W. A. Varady, and H. M. Lindsay, Phys. Rev. Lett. **57**, 595 (1986).
[5]S. H. Chen and J. Teixeira, Phys. Rev. Lett. **57**, 2583 (1986).
[6]B. Cabane, M. Dubois, and R. Duplessix, J. Phys. (Paris) **48**, 2131 (1987).
[7]R. Vacher, T. Woigner, J. Pelous, and E. Courtens, Phys. Rev. B **37**, 6500 (1988).
[8]J. E. Martin and J. P. Wilcoxon, Phys. Rev. A **39**, 252 (1989).
[9]M. Kallala, R. Jullien, and B. Cabane, J. Phys. (France) II **2**, 7 (1992).
[10]B. B. Mandelbrot, *Fractals: Form, Chance, and Dimension* (Freeman, San Francisco, 1977).
[11]R. Jullien and R. Botet, *Aggregation and Fractal Aggregates* (World Scientific, Singapore, 1987).
[12]T. Freltoft, thesis, Riso University, Roskilde, 1986. See also F. Grey and J. K. Kjems, Physica D **38**, 154 (1990).
[13]S. K. Sinha, Physica D **38**, 310 (1990).
[14]M. Foret, J. Pelous, and R. Vacher, J. Phys. (France) I **2**, 59 (1992).
[15]M. Kolb, R. Botet, and R. Jullien, Phys. Rev. Lett. **51**, 1123 (1983).
[16]R. Botet, R. Jullien, and M. Kolb, J. Phys. A **17**, L75 (1983).
[17]R. C. Ball and R. Jullien, J. Phys. (Paris) Lett. **45**, L1031 (1984).
[18]R. Jullien and M. Kolb, J. Phys. A **17**, L639 (1984).
[19]P. Meakin and M. Muthukumar, J. Chem. Phys. **91**, 3212 (1989).
[20]T. Witten and L. Sander, Phys. Rev. Lett. **47**, 1400 (1981).
[21]R. Jullien and P. Meakin, J. Colloid Interface Sci. **127**, 265 (1989).
[22]P. Meakin and R. Jullien, J. Chem. Phys. **89**, 246 (1988).
[23]R. Jullien, A. Pavlovitch, and P. Meakin, J. Phys. A **25**, 4103 (1992).

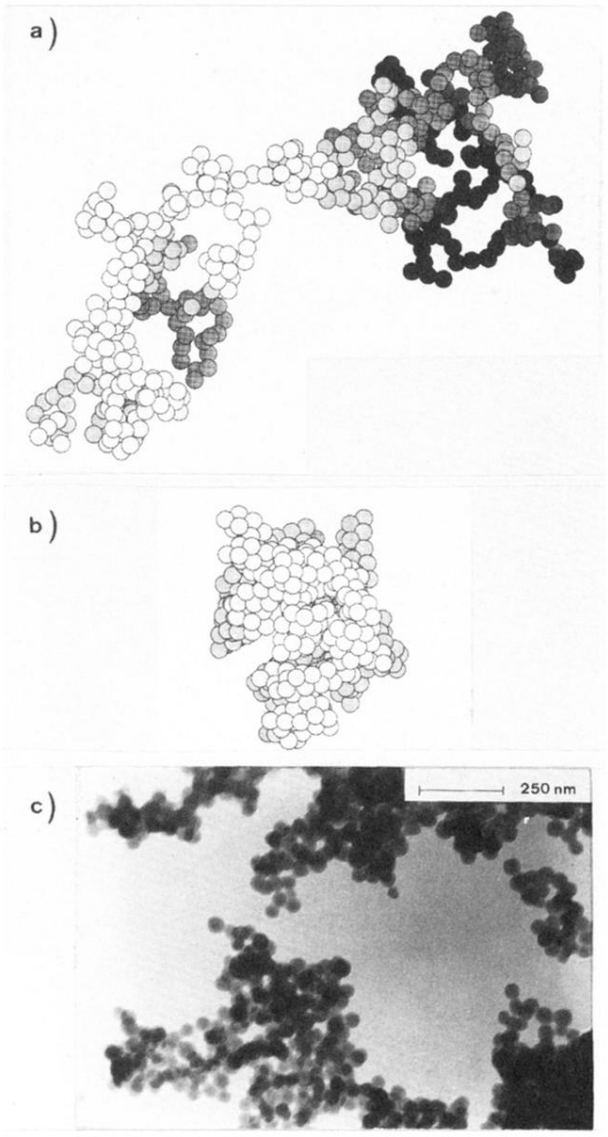

FIG. 1. (a) Three-dimensional aggregate containing 4096 spherical particles built with the ballistic algorithm without restructuring. (b) Same as (a) but with complete restructuring ($R_e = 3$). (c) Micrograph of a 270-Å aerogel sample.